PIER C

(Received 31 July 2024, Accepted 4 October 2024, Scheduled 10 October 2024)

A Novel Single-Layered Dual-Wideband Circularly Polarized Asymmetric Slot Antenna for Wireless Applications

Pradeep Hattihalli Shankaraiah[1, 2], Neelawar Shekar Vittal Shet[1], and Krishnamoorthy Kandasamy[1]

[1]*Department of Electronics and Communication Engineering, National Institute of Technology Karnataka Surathkal, Mangalore, Karnataka 575025, India*
[2]*Department of Electronics and Communication Engineering, Siddaganga Institute of Technology Tumakuru, Karnataka 572103, India*

ABSTRACT: This work focuses on the design and implementation of a dual-wideband asymmetric square-shaped slot radiator with coplanar waveguide (CPW) feed for circular polarization (CP) characteristics. The proposed radiator has inward ground plane extensions in the form of square and rectangular strips on the diagonal corners of the slot. By optimizing the size of strips, a dual-band antenna with CP behaviour is obtained. The inverted L-shaped grounded strip improves axial ratio bandwidth (ARBW). The extended signal line terminated in a wide tuning stub significantly improves impedance bandwidth (IBW) and also further enhances ARBW. The designed asymmetric slot radiator is fabricated using an FR-4 substrate material of dimensions $50 \times 50 \times 1.6\,\text{mm}^3$. This antenna design gives flexibility to alter polarization sense at the dual frequency bands. Further, edge effects are analyzed through electric field distribution, and their impact on impedance and AR characteristics are studied. It is designed, fabricated, and tested, and shows right-hand circular polarization (RHCP) response at 3 GHz and 7.5 GHz in the $+Z$ direction. The experimentally verified results show -10-dB IBWs of 40.12% (range from 2.61 GHz to 3.92 GHz) and 40.21% (range from 6 GHz to 9.02 GHz), and 3-dB ARBWs are 20% (range from 2.70 GHz to 3.30 GHz) and 40.21% (range from 6 GHz to 9.02 GHz) at the resonance bands. The experimentally measured and simulated performance parameters of the prototype are in close agreement. The proposed perturbed slot radiator is well suited for Wi-Fi 6E communication and remote sensing applications.

1. INTRODUCTION

Antennas have a significant role in the field of wireless communication domain. Due to the rapid growth of wireless communication technology, the necessary requirement of antennas with superior features for diverse applications has increased. A modern communication system demands a cost-effective single antenna design, which can perform various functionalities. Many dual-band/multiband antenna designs with linear polarization (LP) can be found in the literature. However, linearly polarized antennas suffer from fading effects, polarization mismatch problems, and multipath propagation effects [1, 2]. Circularly polarized antennas can overcome the drawbacks of LP antennas. Many types of dual-band CP antennas like patch [3], fractal [4], dipole [5], complementary [6], dielectric resonator antenna (DRA) [7], and monopole [8] antennas can be found in the literature. These antennas have complex geometry, low impedance and axial ratio (AR) bandwidths. Many dual-band circularly polarized antennas have been designed using various technologies like substrate integrated waveguide (SIW) [9], metasurface (MTS) [10], and reactive elements based [11]. These designs suffer from complex geometry and fabrication, multilayers, bulkyness, and low bandwidths.

In recent years, wireless communication with multiband applications has made use of planar radiating structures like dual-band slot antennas as they have attractive features like low profile, low conductive loss, conformation, easy fabrication, and broad bandwidth. Different shapes of slot antennas like square [12], rectangular [13], pentagon [14], and hexagonal [15] structures are found in the literature. They are either linearly polarized, restricted to single-band CP or have large dimensions. Some of the CP slot antennas are either single band [16–19], dual polarized [20], or dual feed [21] structures. These designs have single-band CP behavior with low bandwidth. Many CP slot antennas with various feeding methods like CPW feed [22], microstrip feed [23, 24], sequential feed [25], and differential feed [26] are presented in the literature. These works have either complex feed, two-layered designs, or less bandwidths. Among them, CPW feed is simple and supports a single-layered antenna design. Slot antennas of different configurations like open slot [27], narrow slot [28], wide slot [29], annular slot [30], and rotated slot [31] are reported in the literature. They are of either large profile or low axial ratio bandwidth.

A square slot antenna with corner truncation has split ring resonators (SRRs) loaded below the substrate is presented in [32]. The AR bandwidths of 3.1% at 3.1 GHz and 4.2% at 4.7 GHz are achieved. A dual broadband annular CP slot radiator for WLAN applications is reported in [33]. The antenna has

* Corresponding author: Pradeep Hattihalli Shankaraiah (pdeep.hs@gmail.com).

a lightning-shaped slot structure and a crescent-shaped parasitic element in the slot produces dual-band CP radiation. Communication [34] presents a novel corner extended square slot antenna with an inclined copper strip array for CP radiation. In [35], the reported antenna shows dual bands with CP behavior using a single slot structure with an inductor element, a reflector, and a T-shaped microstrip feed. The ARBWs of 6.56% and 7.74% were obtained at 1.227 GHz and 1.575 GHz, respectively. A dual-resonance CP shared-aperture antenna with a SIW slot structure operating in X-band is used as a patch structure with circular polarization radiation in the C-band and is verified experimentally in [36]. ARBWs of 1.04% and 0.75% at 5.77 GHz and 9.3 GHz are respectively reported.

Recently, a slot antenna design having stable in-band gain performance with decreased frequency ratio for dual-band radiation with ARBWs of 1.6% and 2.9% is realized in [37]. In [38], the proposed slot radiator exhibits dual resonances by loading a stub and an inverted L-strip in the ground plane, and ARBWs of 25% and 10.11% are achieved. The design reported in [39] has two orthogonal linear slots cascaded with a non-radiative resonator which results in dual-band CP response with ARBWs of 7.1% and 5.06%.

Due to rapid growth of modern wireless communication, there is a need for Wi-Fi technology that offers faster speeds, lower latency, and improved connectivity for modern applications. Wi-Fi 6E devices are designed to take advantage of the enhanced performance and capacity provided by the 6 GHz band, making them ideal for modern applications that require high-speed connectivity. Designing an antenna with low profile, compactness with simple feed mechanism to achieve dual-band behavior, and wide ARBW for Wi-Fi 6E applications is a challenge.

This article presents a novel low-profile dual resonance asymmetric slot structure with wide ARBW for Wi-Fi 6E communication and remote sensing applications. The diagonal ground plane extensions at the corners of slot, an inverted L-shaped grounded strip, and a vertical tuning stub in the signal line are used to realize a dual wideband CP antenna. It is designed to exhibit CP behavior at resonance bands centered at 3 GHz and 7.5 GHz. The impedance bandwidths (IBWs) are 40.12% and 40.21%, while ARBWs of 20% and 40.21% are achieved at lower and upper resonance bands, respectively. The proposed design is suitable for Wi-Fi 6E devices like standalone routers, laptops, smart TVs, internet of things (IoT) devices, etc.

In the proposed work, three main features have been incorporated within the design: Firstly, inclusion of ground plane extensions at the diagonal opposite corners of slot achieves dual-band CP simultaneously [40]. Secondly, implanting an inverted L-shaped ground strip accounts for the enhancement of ARBW. Lastly, embedding a vertical tuning stub in the extended feed structure results in the enlargement of IBW [41, 42], thereby achieving both wide impedance and AR bandwidths simultaneously. Therefore, a single-layered dual wideband CP slot antenna is achieved with simple feed and less number of design parameters than most of the dual-band CP slot antenna designs in the literature. This confirms the novelty of the proposed design.

The key contributions of the proposed design are:

1. Single-layer, single-feed, and single-radiator design supports dual-band circular polarization characteristics.
2. The design provides wide impedance and AR bandwidths simultaneously.
3. Design flexibility to alter polarization sense by changing the ground plane extensions to other diagonal opposite corners of the slot radiator.
4. Equivalent circuit analysis to validate the $|S_{11}|$ characteristics.
5. Edge effects are analyzed, and their impacts on impedance and AR responses are studied.
6. Compact design with less number of parameters than most of the dual-band CP slot antenna designs in the literature and ease of fabrication.

The rest of the article is organized as follows. Section 2 presents the geometry of the proposed radiator. The evolution steps of the proposed design and surface current flow and electric (E) field distributions are described in Section 3. The parametric study, equivalent circuit model, and edge effects are presented in Section 4. Section 5 compares the experimentally measured and simulated performance parameters. Finally, Section 6 concludes the paper.

2. ANTENNA DESIGN

This proposed design is a circularly polarized dual wideband asymmetric slot radiator using a cost-effective FR-4 substrate material of size $50 \times 50\,\text{mm}^2$, relative permittivity $(\varepsilon_r) = 4.4$, and substrate thickness $(h) = 1.6\,\text{mm}$ with loss tangent $(\tan\delta) = 0.025$. A square-shaped slot etching is performed on the dielectric material, fed by a CPW feed line. Figs. 1(a) and (b) illustrate the top sight and side sight of the proposed geometric configuration, respectively. The proposed design comprises an asymmetric slot radiator with the perturbation introduced in the form of inward ground plane extensions at the diagonal opposite corners of a conventional slot radiator in square and rectangular strips. The ground plane extensions on the upper left and lower right corners of the slot are of dimensions $(S_{L1} \times S_{W1})$ and $(S_{L2} \times S_{W2})$, respectively. Further, an inverted L-shaped strip on the ground plane has lengths and widths $(L_1 \times W_1$ and $L_2 \times W_2)$. A wide vertical tuning stub on the extended signal line has dimensions $(L_t \times W_t)$.

The performance of the CP slot antenna, particularly the AR feature, will be impacted by the size of the ground plane. As a result, it is required to make sure that the ground and slot have the right size. The suggested work's optimal design has a fixed L/Ls ratio of 1.123.

According to the simulation results, selecting ground plane extensions with the following dimensions: $S_{L1} = S_{W1} = 13\,\text{mm}$ ($\sim 0.292Ls$), $S_{L2} = 27\,\text{mm}$ ($\sim 0.606Ls$), $S_{W2} = 17\,\text{mm}$ ($\sim 0.382Ls$) improves IBW in addition to increasing ARBW.

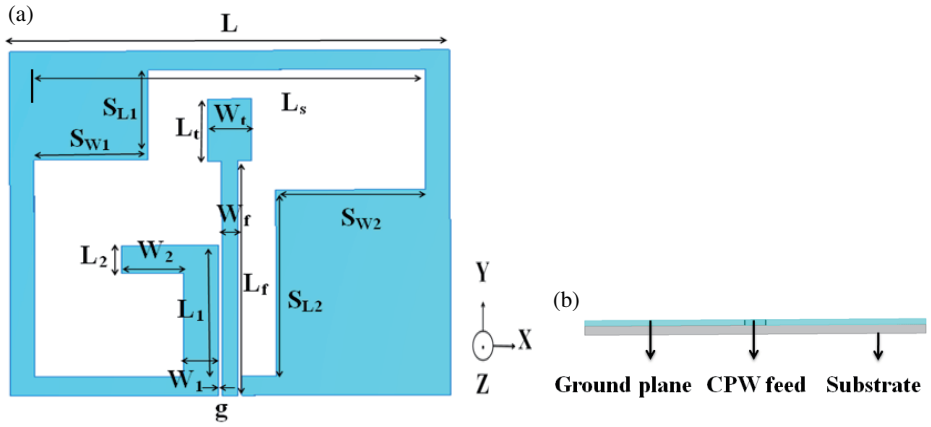

FIGURE 1. Geometry of the proposed design (a) Top vision, (b) Side vision (Optimized dimensions in mm: $L = 50$, $L_s = 44.5$, $S_{L1} = 13$, $S_{W1} = 13$, $S_{L2} = 27$, $S_{W2} = 17$, $L_t = 9$, $W_t = 7$, $L_f = 34$, $W_f = 2.8$, $L_1 = 19$, $L_2 = 4$, $W_1 = 4$, $W_2 = 7$, $g = 0.25$).

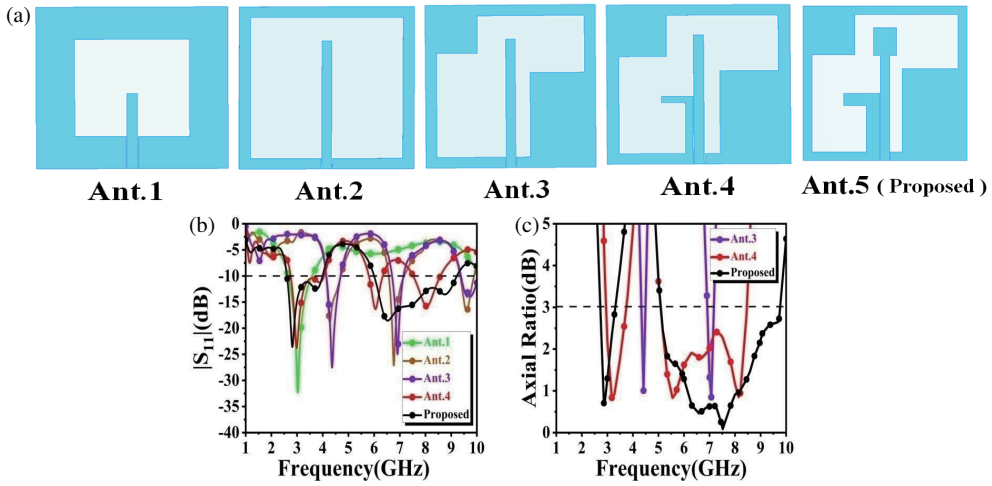

FIGURE 2. (a) Evolution stages to realize the proposed radiator. (b) $|S_{11}|$ characteristics. (c) Axial ratio values.

3. ANTENNA WORKING PRINCIPLE

This segment describes the operating principle of the proposed radiator using the design evolution steps and CP mechanism.

3.1. Design Evolution

Figure 2(a) depicts the realization of a dual resonance antenna structure with the aid of various antenna prototypes. The simulated plots of S-parameter characteristics and AR magnitudes for different prototypes and the proposed design are illustrated in Figs. 2(b) and (c).

Ant. 1: This structure is a wide slot antenna with CPW feed and linear polarization characteristics. The conventional square slot antenna radiates at its fundamental transverse electric mode (TE_{10}), and its resonance is determined using [43],

$$f_r = \frac{c}{2L_s}\sqrt{\frac{2}{1+\in_r}} \tag{1}$$

where L_s represents the slot length, and ε_r denotes the relative permittivity of the dielectric material. With this prototype, the axial ratio is quite large ($>$ 30 dB). Fig. 2(b) shows that the conventional slot structure resonates at 3 GHz.

Ant. 2 (Dual-band generation): With the extension of slot dimensions and length of the feed line, dual resonances at 4.3 GHz and 6.8 GHz are obtained with no circular polarization. Dual-band response in a square slot antenna with an extended CPW feed line as well as slot dimensions is achieved by carefully designing both slot and feed line to support multiple resonant frequencies. Extending the slot introduces higher order modes TE_{20}, TE_{30} and so on, which resonate at frequencies above the fundamental mode and are characterized by additional current paths within the slot structure, while the extended CPW feed line influences the impedance matching and excitation of multiple frequencies by modifying its electrical length. Fine tuning the length of the CPW feed line and the dimensions of the slot allows for better coupling between them and generation of mixed-mode resonances. These resonances are a combination of fundamental and higher-order modes, often resulting in dual-band or multi-band behavior.

Ant. 3 (CP mechanism): Asymmetry in the conventional slot antenna is produced by the placement of ground plane ex-

TABLE 1. Performance comparison of different prototypes and the proposed slot radiator.

Prototypes	IBW	ARBW	Modifications in the geometry
Ant. 1	2.64 GHz–3.58 GHz, 30.22%	—	Conventional slot
Ant. 2	4.13 GHz–4.69 GHz, 12.69% 6.57 GHz–7.14 GHz, 8.31% 9.37 GHz–9.90 GHz, 5.50%	—	Extension of Slot and feed line dimensions (Ls, L_f)
Ant. 3	4.17 GHz–4.72 GHz, 12.37% 6.68 GHz–7.16 GHz, 6.93%	4.33 GHz–4.49 GHz, 3.62% 6.91 GHz–7.16 GHz, 3.55%	Inclusion of ground plane extensions ($S_{L1} \times S_{W1}$) & ($S_{L2} \times S_{W2}$)
Ant. 4	2.75 GHz–4.04 GHz, 38% 5.79 GHz–6.33 GHz, 8.91% 7.52 GHz–8.56 GHz, 12.93%	2.94 GHz–3.74 GHz, 23.95% 5.79 GHz–6.33 GHz, 8.91% 7.52 GHz–8.46 GHz, 11.76%	Placement of inverted L-shaped ground strip ($L_1 \times W_1$, $L_2 \times W_2$)
Ant. 5 (Proposed)	2.60 GHz–4 GHz, 42.42% 6 GHz–9.22 GHz, 42.31%	2.69 GHz–3.31 GHz, 20.66% 6 GHz–9.22 GHz, 42.31%	Termination of feed line with vertical tuning stub ($L_t \times W_t$)

tensions. The inclusion of ground plane extensions [40] perturbs the slot's current distribution, influencing the resonant modes and their phase relationships within the slot. Fine tuning the length of the CPW feed line and the dimensions of the slot allows for the excitation of degenerate modes TE_{10} and TE_{01}, TE_{20}, and TE_{02}, which are orthogonal to each other with quadrature phase difference. As a result, the superposition of these orthogonal modes produces a rotating electric field vector, which is the characteristic of circular polarization. This prototype radiates RHCP waves at two distinct narrow bands 4.4 GHz and 7 GHz.

Ant. 4 (Wide 3-dB AR bands): Both the TE_{02} and TE_{20} modes are inherently narrowband which can generate CP in slot antennas. Achieving wideband performance typically requires additional design techniques like optimizing slot dimensions, employing effective feeding techniques, etc. In the proposed design, the slot geometry is modified by embedding an inverted L-shaped ground strip. This introduces additional resonant modes for a wider range of frequencies while maintaining CP. The coupling between the feed line and inverted L-shaped ground strip perturbs the current distribution in the slot structure so that the 3-dB AR bands are shifted to lower frequencies, while enhancing the 3-dB ARBWs. Implanting inverted L-shaped ground strip in the slot structure leads to a large ARBW and may not guarantee satisfying impedance matching [41, 42]. Fig. 2(c) shows that there is a significant increase in the ARBW which is noticed due to the inverted L-shaped ground strip.

Ant. 5 (Proposed) (Wide-band response): Finally, a vertical tuning stub is embedded in the feed line to widen the impedance band. Appropriate design of tuning stub results in combining two higher order resonances to form a wider impedance band so as to completely cover the 3-dB AR band. The vertical tuning stub has effectively widened the VSWR $\leq$ 2 impedance band apart from slightly broadening the 3-dB AR band [41, 42]. This is the optimized proposed design, which significantly improves both IBW and ARBW performances simultaneously. Furthermore, a dual wideband CP slot antenna is achieved.

The simulated results in terms of IBW and ARBW of different prototypes and the proposed slot configuration are summarized in Table 1.

The simulation results in Table 1 indicate that no CP resonances were contributed by Ant. 1 and Ant. 2 prototypes. It can be inferred from Ant. 3's response that the inclusion of ground plane extensions into the slot radiator generates two CP bands. Embedding an inverted L-shaped ground strip enhances ARBW performance based on the output of prototype Ant. 4. Finally, the proposed configuration leads to the conclusion that the suggested slot radiator's ARBW is significantly increased by terminating the feed line with a vertical tuning stub, which primarily improves IBW performance. Comparing the performances of dual-band CP prototype Ant. 3 and the proposed design, there is a large improvement of IBW from 9.65% to 42.36% and ARBW from 3.58% to 31.48% on average.

3.2. CP Mechanism

In this subsection, the mechanism of CP generation of the proposed design is explained by simulated distribution of surface current. Further, the change of CP sense is discussed by simulated electric field distribution.

This subsection illustrates CP generation of the proposed structure by observing the flow of vector surface current on the slot structure, feed line, and strips at different phases obtained from simulations at resonance bands. The current distributions for phases $\omega t = 0°$, 90°, 180°, and 270° at 3 GHz and 7.5 GHz are observed in the positive Z-direction on the XY-plane as depicted in Figs. 3(a) and (b). From the observations, the distributed surface current vector rotates counterclockwise as the phase progresses from 0° to 270°. Hence, the proposed antenna radiates RHCP waves at both resonant frequencies. CP operation is obtained on the excitation of asymmetric slot structure. The flow direction of the surface current is reversed due to altering the position of ground plane extensions to other diagonal opposite corners of slot radiator. Therefore, in this case, the

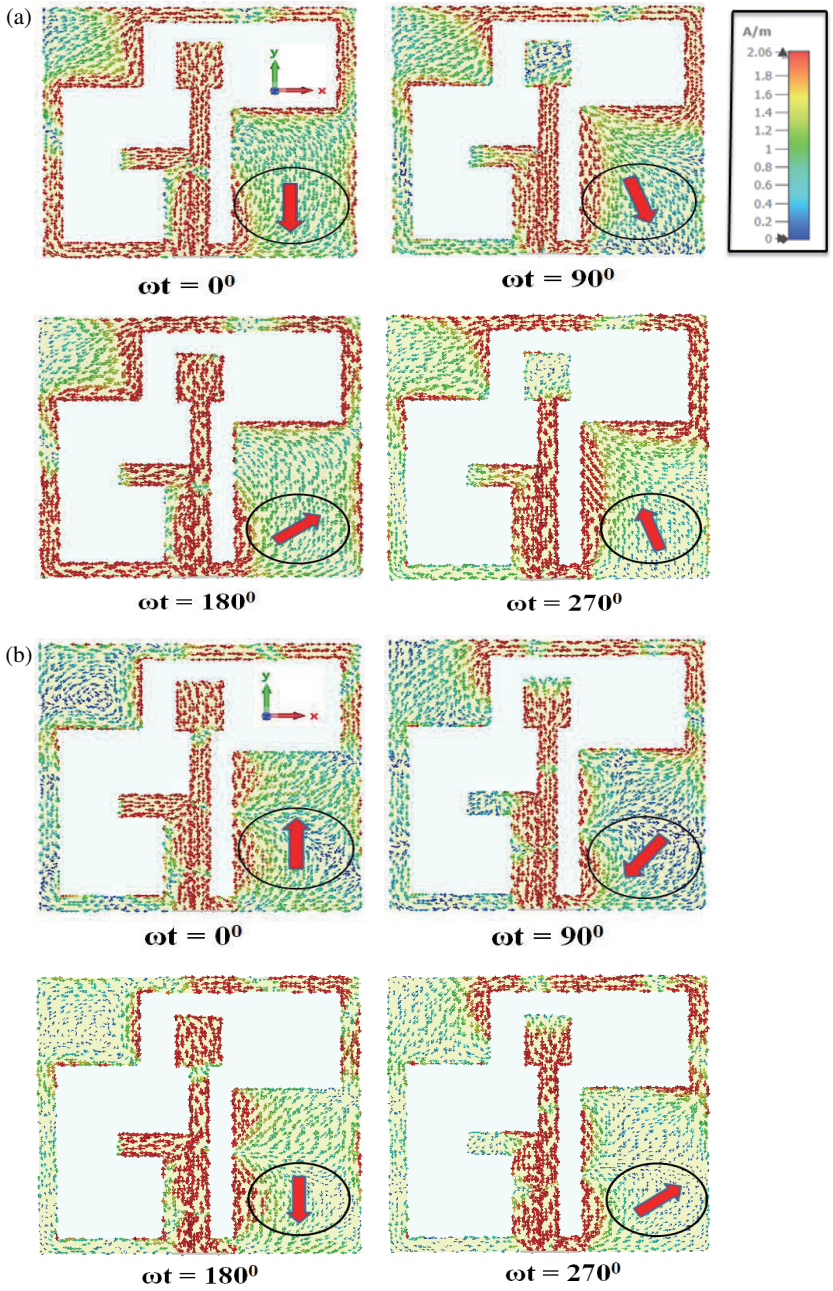

FIGURE 3. Vector surface current behaviour on simulation at center frequencies: (a) 3 GHz, (b) 7.5 GHz.

antenna radiates left hand circular polarization (LHCP) waves at its resonance bands.

The change in the sense of CP behaviour of asymmetric slot radiator can be illustrated by analyzing the simulation results of distributed electric (E) fields along the positive Z-direction on the XY-plane. Considering the mirror of the proposed design along the x-axis, the inward ground plane extensions appear at the other opposite diagonal corners of the slot radiator (as in Fig. 4) which results in LHCP behaviour at both the bands of operation. Figs. 4(a) and (b) illustrate the simulation results of E-field behaviour of the dual-band slot radiator for LHCP radiation at resonance frequencies for the phases $\omega t = 0°$ and $\omega t = 90°$.

4. ANTENNA ANALYSIS

This section discusses the analysis of the proposed design using the equivalent circuit model, parametric study and edge effects.

4.1. Equivalent Circuit Analysis

The circuit simulation is carried out using Advanced Design System (ADS) simulation software. The circuit representing CPW fed slot antenna shown in Fig. 5(a) consists of lumped components R_f, L_f, and C_f, which represent the sub-miniature version A (SMA) connector and coplanar waveguide feed. The slot structure is represented by the parallel combination of L_s and C_s.

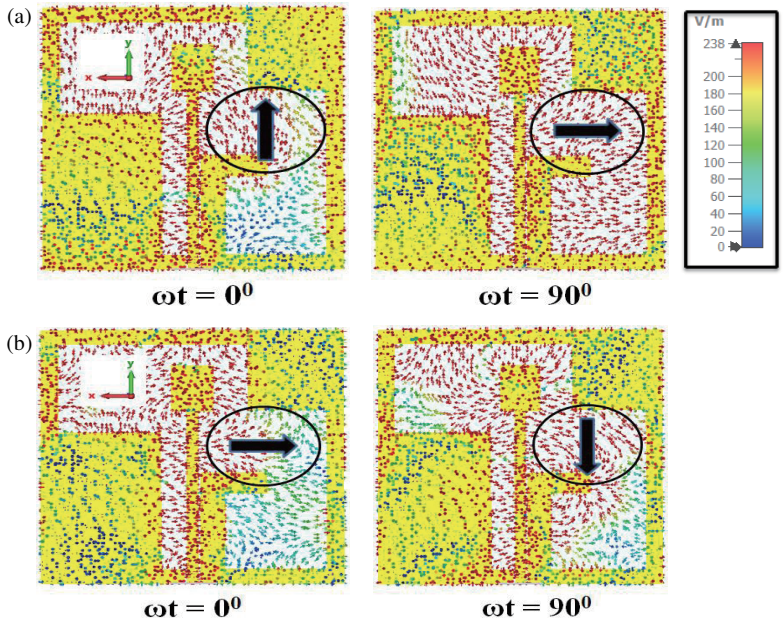

FIGURE 4. Simulated E-field behaviour for LHCP waves at resonances: (a) 3 GHz, (b) 7.5 GHz.

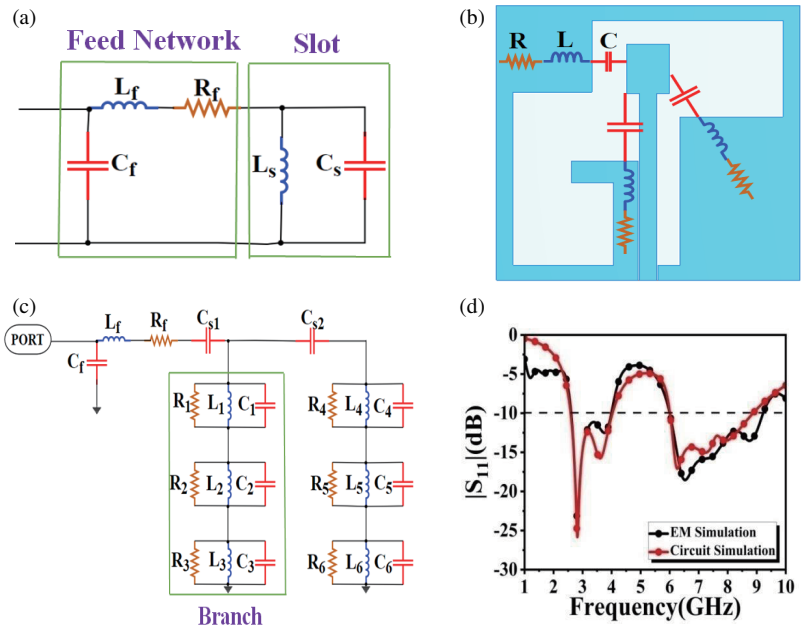

FIGURE 5. Circuit equivalent modeling of the proposed work: (a) CPW fed slot antenna. (b) Antenna circuit model with three RLC resonant circuits. (c) Equivalent circuit diagram of the proposed CPW fed Asymmetric slot antenna. (d) Comparison of reflection coefficient plots.

To achieve asymmetric slot radiator, the inclusion of inward ground plane extensions at the diagonal opposite corners of a conventional slot radiator in the form of square and rectangular strips and their coupling to tuning stub is represented by two RLC resonant circuits. The third RLC resonant circuit represents the coupling of inverted L-shaped ground strip to tuning stub, which is depicted in Fig. 5(b), showing antenna circuit model with three RLC resonant circuits. This is represented by a branch composed of three parallel RLC resonant cavities in a series connection in Fig. 5(c).

To achieve dual-frequency bands, two branches of three parallel RLC resonant cavities in a series connection is represented in Fig. 5(c), which depicts the circuit equivalent transmission line representation of the proposed dual resonance CP slot radiator. Capacitances C_{s1} and C_{s2} represent the slot coupling.

Figure 5(d) illustrates the comparison of reflection coefficient plots obtained due to the circuit and EM simulations. The S-parameter simulation results obtained are in close agreement with the extracted circuit parameter values. The discrete parameter values of the circuit model obtained after rigorous sim-

ulations are $R_1 = 181.75\,\Omega$, $L_1 = 1.4\,\text{nH}$, $C_1 = 0.305\,\text{pF}$, $R_2 = 600.9\,\Omega$, $L_2 = 0.20\,\text{nH}$, $C_2 = 2.18\,\text{pF}$, $R_3 = 5\,\text{K}\Omega$, $L_3 = 0.6\,\text{nH}$, $C_3 = 1.30\,\text{pF}$, $R_4 = 14\,\Omega$, $L_4 = 40\,\text{nH}$, $C_4 = 1.50\,\text{pF}$, $R_5 = 535\,\Omega$, $L_5 = 3.40\,\text{nH}$, $C_5 = 1.40\,\text{pF}$, $R_6 = 76\,\Omega$, $L_6 = 1\,\text{nH}$, $C_6 = 1.55\,\text{pF}$, $R_f = 19.90\,\Omega$, $L_f = 1.3\,\text{nH}$, $C_f = 5 \times 10^{-5}\,\text{pF}$, $C_{s1} = 0.705\,\text{pF}$, $C_{s2} = 5.87\,\text{pF}$.

4.2. Parametric Analysis

The parametric study is carried out to know the sensitivity of impedance performance and axial ratio bandwidth of the resonance bands by varying physical parameters of the antenna. In this analysis, a single parameter value is varied, whereas the rest of the parameters of the antenna are kept constant at a final optimized value. The key parameters of this antenna design are corner strip width (S_{W1}), inverted L-shaped ground strip length (L_2), slot length (L_s), and substrate thickness (h).

4.2.1. Corner Strip width (S_{W1})

Figure 6(a) shows the simulation plots of $|S_{11}|$ characteristics and AR response for varying values of corner strip width S_{W1}. The asymmetry produced in a conventional slot structure due to corner strips is responsible for CP characteristics. There is a slight increase in the IBW of the upper band due to an increase in the strip width. It mainly influences the widening of the AR bandwidth. With the increase of S_{W1}, the lower resonance band slightly shifts to the higher resonance frequency side, and AR $< 1\,\text{dB}$ is achieved. ARBW increases greatly in the higher resonance band compared to the lower frequency band. Therefore, the final optimized value $S_{W1} = 13\,\text{mm}$ is considered in the proposed design.

4.2.2. Inverted L-Shaped Ground Strip Length (L_2)

Figure 6(b) depicts the simulated plots of $|S_{11}|$ values and AR curves for varying values of inverted strip length L_2. As the length of the inverted ground strip increases, the lower resonance band moves slightly towards lower frequency side. ARBW in the upper band improves greatly, and AR of less than 1 dB is achieved. Therefore, the final optimized value $L_2 = 4\,\text{mm}$ is considered in the proposed design.

4.2.3. Slot Length (L_s)

Figure 6(c) depicts the simulated plots of $|S_{11}|$ parameter values and AR curves for varying values of slot dimension L_s. As the slot size decreases, the resonance bands shift slightly towards higher frequency. There is slight improvement in the IBW of resonance bands by reducing the slot dimension from 46.5 mm to 44.5 mm. Decreasing the slot size has greater influence on the ARBW performance of dual resonance bands. ARBWs of 11.85%, 16.57%, and 20.66% for lower resonance band and 20.47%, 41.76%, and 42.31% for upper frequency band are achieved for decreasing values of slot dimension $L_s = 46.5\,\text{mm}$, 45.5 mm, and 44.5 mm, respectively. Therefore, the final optimized value $L_s = 44.5\,\text{mm}$ is considered in the proposed design.

4.2.4. Substrate Thickness (h)

Figure 6(d) depicts the simulated plots of $|S_{11}|$ values and AR curves for varying values of substrate thickness h. As the thickness of the substrate increases, the resonance bands slightly move towards the lower frequency side. ARBW improves significantly for the upper resonance band. ARBWs of 30.43%, 38.94%, and 42.31% are achieved for substrate thicknesses $h = 0.8\,\text{mm}$, 1 mm, and 1.6 mm, respectively, for the upper resonance band. Therefore, the final optimized value $h = 1.6\,\text{mm}$ is considered in the proposed design.

4.3. Analysis of Edge Effects

Edge effects play a crucial role in determining the performance of antennas. These effects in slot radiator are the phenomena that occur at the boundaries of the slot, which can significantly impact the antenna's performance, including its radiation patterns, impedance, and bandwidth. Field distribution tends to concentrate near the edges of the slot and ground plane. This nonuniform field distribution can lead to variations in radiation characteristics. Fig. 7 shows field distribution for different sizes of ground plane. In order to minimize these edge effects, techniques like rounding or tapering edges, optimizing slot dimensions, and ensuring a sufficiently large ground plane can be employed. In the proposed work, by careful design and analysis, edge effects are minimized through optimizing the slot geometry, while at the same time large bandwidth is achieved.

Figure 8 depicts the effects of ground plane variation on bandwidth performance of the proposed design. The decrease in ground plane's size shifts the impedance bands toward lower frequency side. Further, 3-dB AR band for higher resonance band becomes narrower to a greater extent. The increase in ground plane's size moves the impedance bands toward higher frequency range [44], and the impedance bands become narrower. This is due to different near-field distributions for different sizes of the ground plane. As a result, the amount of overlap of impedance band with 3-dB AR band for resonance bands decreases, thereby, affecting the CP center frequencies of the slot antenna. Hence, the operating frequencies of the slot radiator are dependent on ground plane's size. Table 2 depicts the effects of variation of ground plane's size on impedance and AR bandwidths performance.

From Fig. 7, it can be inferred that with the increase in ground plane size to $53\,\text{mm} \times 53\,\text{mm}$, edge effects are minimized. However for this ground plane's size, from Table 2, it is observed that the achieved impedance and AR bandwidths become less. There is a trade-off between bandwidth performance and edge effects. In order to enhance IBW and ARBW and also with reduced edge effects, the ground plane size of $50\,\text{mm} \times 50\,\text{mm}$ is considered in the proposed design.

5. RESULTS AND DISCUSSION

The simulation and fabrication of the dual-wideband asymmetric square slot radiator were performed using the CST microwave studio software and S103 LPKF PCB prototyping machine, respectively. The proposed design with the final optimized physical dimensions was fabricated and experimentally

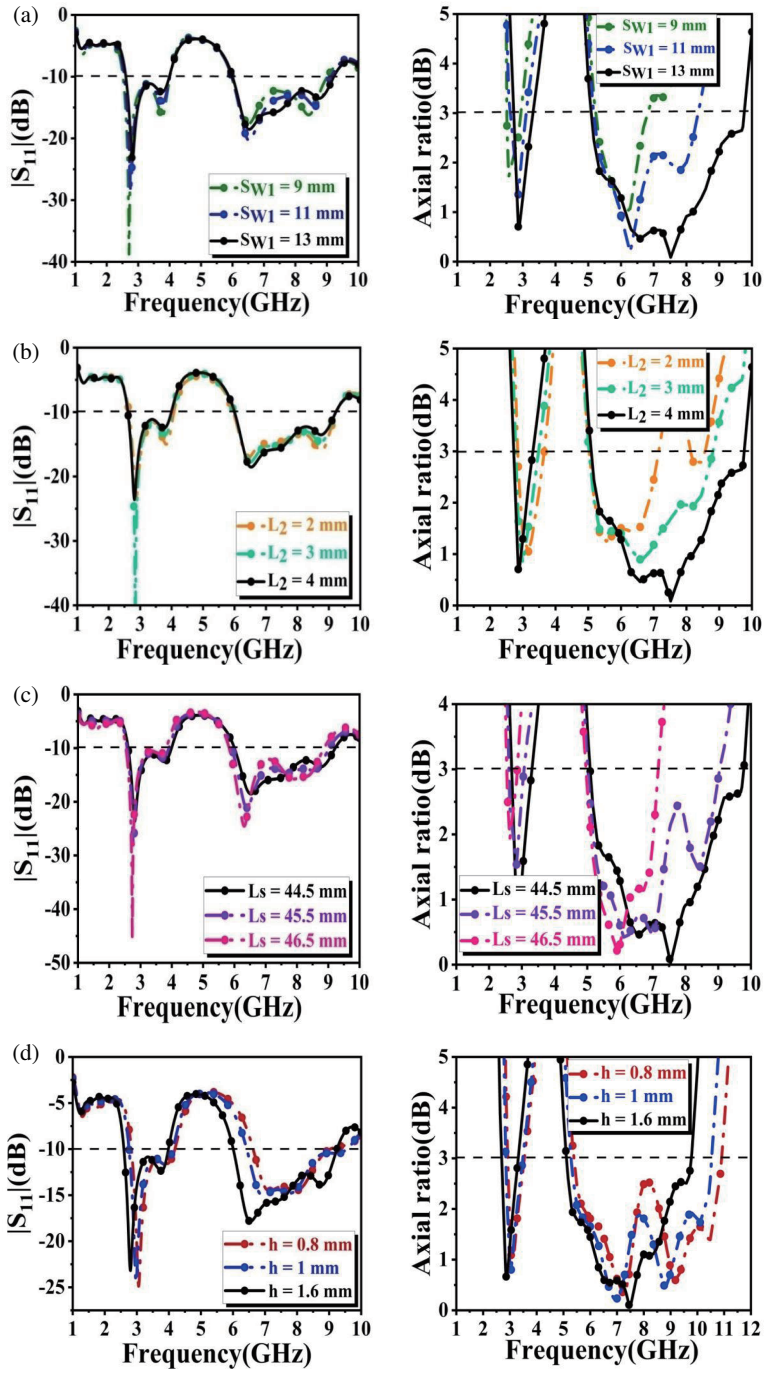

FIGURE 6. $|S_{11}|$ performance and axial ratio values for (a) S_{W1} variation, (b) L_2 variation, (c) L_s variation, (d) h variation.

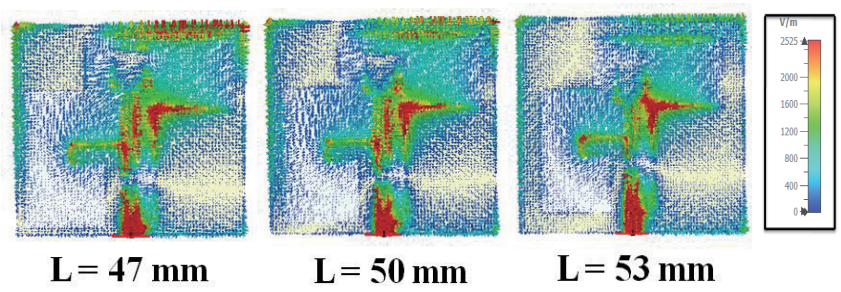

FIGURE 7. Field distribution showing edge effects for different sizes of ground plane.

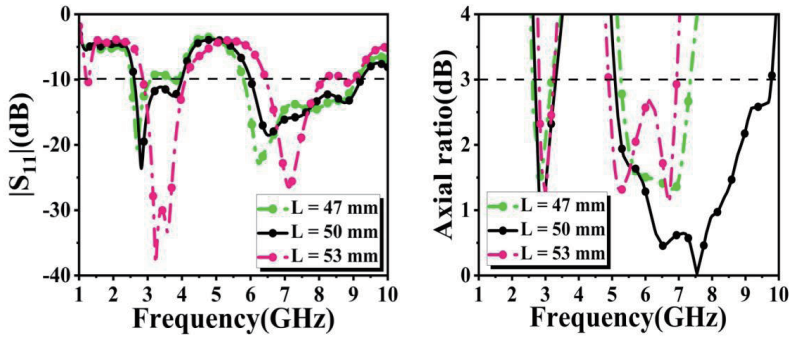

FIGURE 8. Impedance and AR characteristics for ground plane variation.

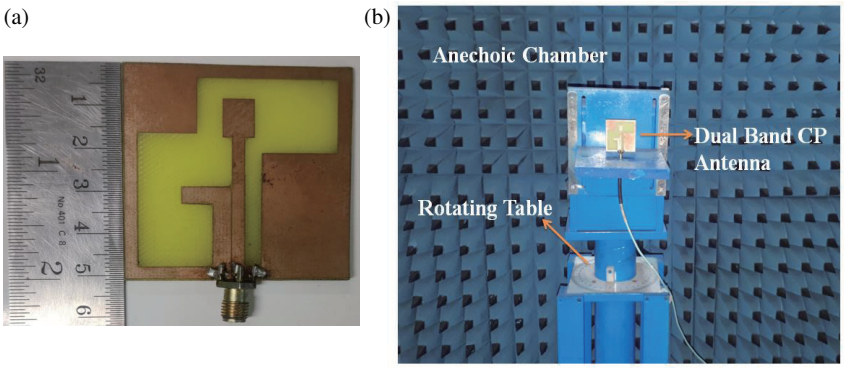

FIGURE 9. (a) Fabricated antenna prototype. (b) Measurement setup.

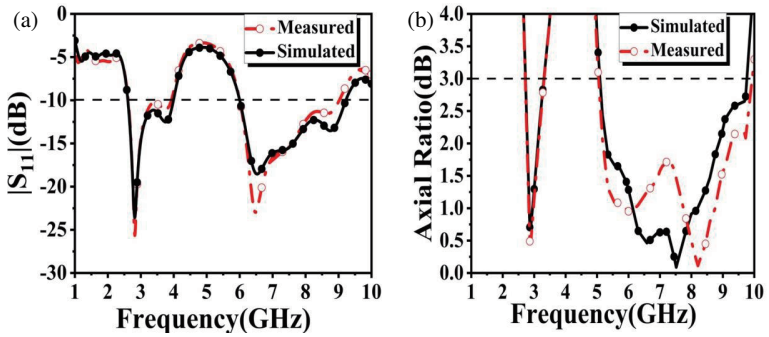

FIGURE 10. Simulation and experimental results. (a) S-parameter values. (b) AR response.

TABLE 2. Effects of variation of ground plane's size on impedance and AR bandwidths performance.

Size of the ground plane ($L \times L$) mm^2	Bandwidth	
	Impedance (%)	Axial ratio (%)
47 × 47	20, 44.35	16.52, 23.61
50 × 50	42.42, 42.31	20.66, 42.31
53 × 53	35.39, 23.31	12.45, 7.32

measured to validate the simulation results. Figs. 9(a) and (b) show a photograph of the fabricated design prototype and measurement setup.

Agilent N9918A Vector Network Analyzer (VNA) was used for $|S_{11}|$ measurement. The experimentally determined and simulated values of performance parameters are in close agreement. There are small deviations between the two results due to fabrication errors.

Figures 10(a) and (b) depict the $|S_{11}|$ response and axial ratio behaviour, respectively, obtained from the simulation and experiment of the proposed radiator.

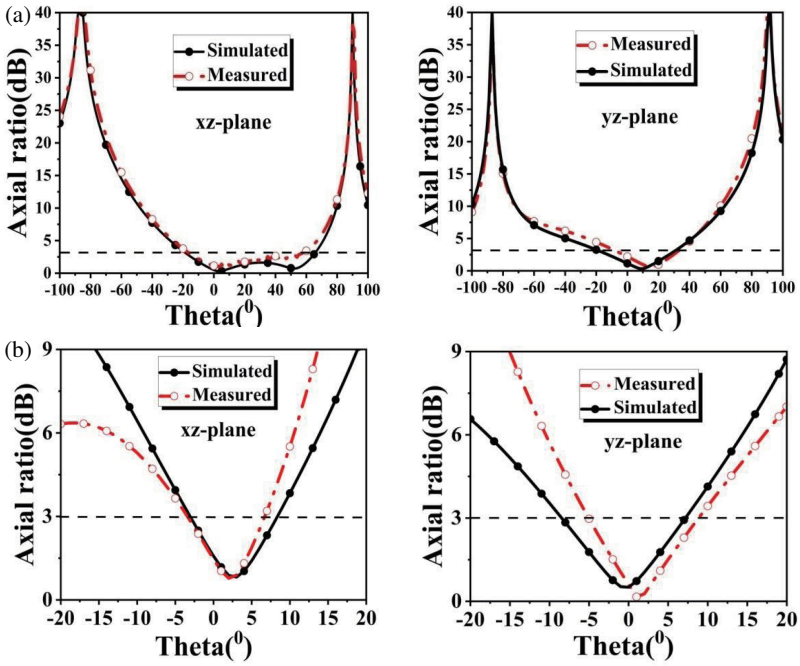

FIGURE 11. Comparison of AR beamwidth plots at resonances: (a) 3 GHz, (b) 7.5 GHz.

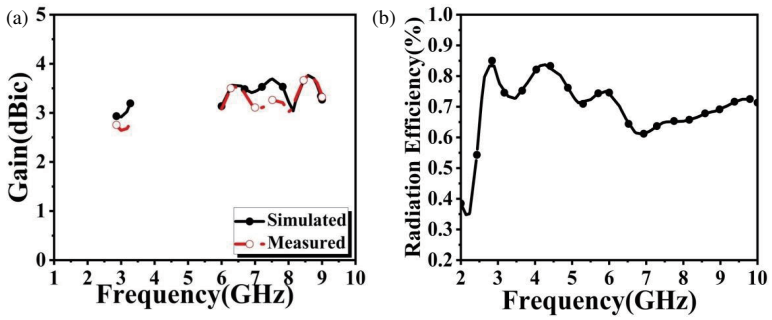

FIGURE 12. Simulation and measurement plots of: (a) Peak gain, (b) Simulated Radiation efficiency.

The simulated and measured $|S_{11}| < -10$-dB BWs for the lower frequency band are 42.42% (range from 2.60 GHz to 4 GHz) and 40.12% (range from 2.61 GHz to 3.92 GHz), and for the higher resonance band, the BWs are 42.31% (range from 6 GHz to 9.22 GHz) and 40.21% (range from 6 GHz to 9.02 GHz), respectively. The simulated and experimentally measured 3-dB ARBWs for lower resonance band are 20.66% (range from 2.69 GHz to 3.31 GHz) and 20% (range from 2.70 GHz to 3.30 GHz), and for the higher resonance band, the BWs are 42.31% (range from 6 GHz to 9.22 GHz) and 40.21% (range from 6 GHz to 9.02 GHz), respectively.

The AR as a function of elevation angle of the proposed slot radiator at 3 GHz and 7.5 GHz is plotted in Fig. 11. The measured 3-dB AR beamwidths of 73.3° and 40.1° at 3 GHz and 10.3° and 14.1° at 7.5 GHz are obtained in the xz-plane and yz-plane, respectively.

Figures 12(a) and (b) depict the experimental and simulated plots of CP gain and simulated radiation efficiency of the dual-band radiator. The simulated values of peak gains of 2.91 dBic at 3 GHz and 3.68 dBic at 7.5 GHz are obtained, whereas experimentally measured values of peak gains of 2.64 dBic at 3 GHz and 3.26 dBic at 7.5 GHz are obtained. The simulated radiation efficiency values of 78.93% at 3 GHz and 64.96% at 7.5 GHz are obtained.

The proposed antenna radiation performance was measured using a near-field anechoic chamber. Figs. 13(a) and (b) depict the simulated and experimentally measured radiation patterns of the dual-band slot design in two principal planes (XZ and YZ) at operating frequencies of 3 GHz and 7.5 GHz, respectively. The RHCP wave is observed for dual resonances in the positive Z-direction. The figure illustrates that the antenna radiation is bidirectional in nature and in close agreement with the simulated and experimentally measured co-pol and cross-pol levels in both resonance bands.

It can be seen from the radiation patterns that the LHCP level falls -15 dB below the RHCP level in the lower resonance band and -20 dB at the upper resonance band. RHCP is obtained at a maximum inclined angle of $-17°$ (YZ-plane) and $+16°$ (YZ-plane) with respect to broadside direction at the first and second

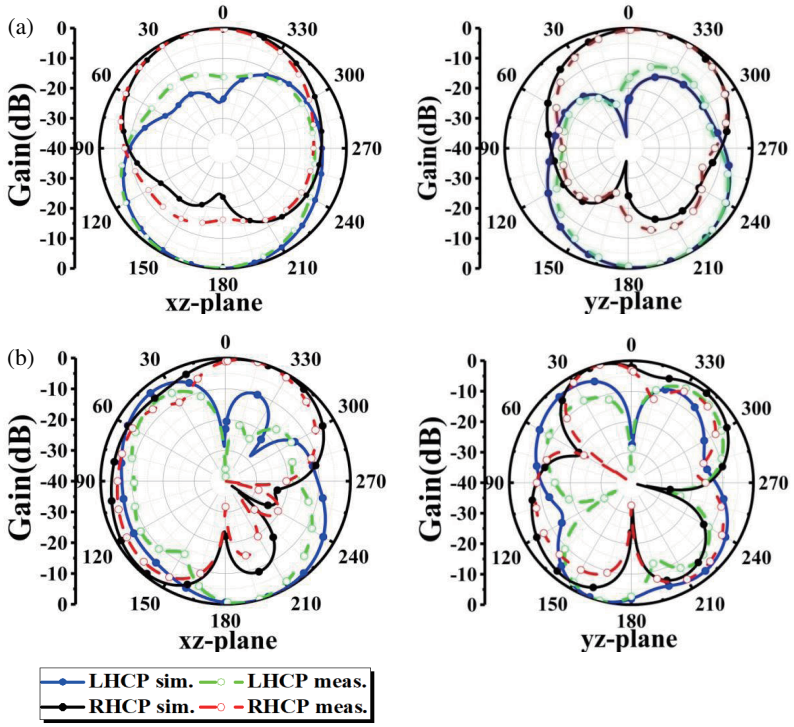

FIGURE 13. Comparison of radiation plots at resonances: (a) 3 GHz, (b) 7.5 GHz.

TABLE 3. Comparative analysis of this work with other similar kinds of CP slot antennas in the literature.

Ref. No.	Electrical Size	Res. Freq. (GHz)	IBW (%)	ARBW (Band) (%)	ARBW (Beam) (°)	CP Gain (dBic)	CP Sense change (RHCP/ LHCP)	Eq. Circuit Analysis
[17]	$0.97\lambda_o \times 0.97\lambda_o$	5.8	3.6	—	68/57	10.75	No	No
[18]	$0.69\lambda_o \times 0.69\lambda_o$	5.73	1.63	0.44	70/104	7.96	No	No
[19]	$0.7\lambda_o \times 0.7\lambda_o$	3.45	18.6	9.5	176/147	7.65	No	No
[24]	$0.41\lambda_o \times 0.41\lambda_o$	2.5, 5.5	114.7	60.2, 32.7	——	4.2, 3.4	Yes	No
[29]	$0.37\lambda_o \times 0.32\lambda_o$	1.75, 3.3	26.04, 18.93	22.22, 10.53	——	3.6, 1.5	No	No
[31]	$0.31\lambda_o \times 0.31\lambda_o$	1.88, 4.41	24.3, 33.4	4.4, 7.9	——	1.72, 2.17	No	No
[32]	$0.72\lambda_o \times 0.72\lambda_o$	3.1, 4.7	12.9, 8.5	3.1, 4.2	——	7.3, 8.5	Yes	Yes
[33]	$0.4\lambda_o \times 0.48\lambda_o$	2.4, 5.5	25.9, 25.9	13.3, 16.9	——	2.3, 3.1	No	No
[34]	$0.4\lambda_o \times 0.4\lambda_o$	2.4, 4.2	42.4, 15.6	45.5, 15.7	——	3.8, 4.5	Yes	No
[35]	$0.33\lambda_o \times 0.33\lambda_o$	1.22, 1.57	40.57	6.56, 7.74	——	7.72, 8.11	No	No
[36]	$0.86\lambda_o \times 0.86\lambda_o$	5.77, 9.3	4.5, 2.7	1.04, 0.75	——	8.4, 6.35	No	No
[37]	$0.45\lambda_o \times 0.42\lambda_o$	1.88, 2.39	35.6	1.6, 2.92	——	2.8, 3.5	No	No
[38]	$0.45\lambda_o \times 0.45\lambda_o$	5, 12.5	75.70, 32	25, 10.11	——	3.8, 5	No	No
[39]	$0.99\lambda_o \times 0.99\lambda_o$	2.46, 3.12	35.48, 25	7.1, 5.06	——	3.36, 3.16	No	Yes
PW	$0.5\lambda_o \times 0.5\lambda_o$	3, 7.5	40.12, 40.21	20, 40.21	73.3/40.1, 10.3/14.1	2.64, 3.26	Yes	Yes

IBW: Impedance Bandwidth; ARBW (Band): Axial ratio bandwidth; ARBW (Beam): Axial ratio beamwidth for ($\varphi = 0°/90°$); PW: Proposed work. Where λ_0 is free space wavelength corresponding to lowest resonance frequency.

resonance bands, respectively. This inclination of the beam is because of the asymmetry of the slot radiator.

Table 3 gives the comparative analysis of the proposed design with other similar CP slot antennas found in the literature.

The single-band CP designs realized in [17–19] have larger dimensions, less bandwidths, larger AR beamwidths, and CP gains, whereas dual-band CP designs reported in [29, 37, 38] have less impedance and AR bandwidths than the proposed work. Dual-band slot radiators realized in [24, 31, 34] are two-layered designs with less bandwidths than the proposed design, whereas a SIW based slot radiator designed with two substrates and dual ports is presented in [36]. The antenna reported in [33] has complex geometry, and that in [35] has complex feed, showing less bandwidths than the proposed design, and CP polarization sense cannot be altered. The works described in [32, 39] have either larger dimensions or large profile compared to the proposed design. The desirable features of the proposed radiator are low profile, compactness, sense of polarization change, wide impedance and AR bandwidths compared to other slot antenna designs found in the literature.

6. CONCLUSION

A dual resonance perturbed square-shaped slot radiator with a simple design for CP radiation is presented in this article. The proposed antenna is fabricated and measured in terms of IBW, ARBW, AR beamwidth, peak gain, and radiation patterns. Good agreements have been observed between the experimentally measured and simulated results. The experimentally obtained IBWs for $|S_{11}| < -10$ dB at two working bands are 40.12% (range from 2.61 GHz to 3.92 GHz) and 40.21% (range from 6 GHz to 9.02 GHz). The 3-dB axial ratio BWs are 20% (range from 2.70 GHz to 3.30 GHz) and 40.21% (range from 6 GHz to 9.02 GHz). Parametric study, equivalent circuit analysis, and the mechanism of CP generation were carried out at the resonance bands. The design has the flexibility to alter the polarization sense by changing the position of ground plane extensions to other diagonal opposite corners of the slot radiator. This slot design fits for Wi-Fi 6E communication and remote sensing applications. In summary, this antenna design is suitable for modern wireless communication systems for dual wideband CP radiation as it offers compactness with wide impedance and axial ratio BWs compared to other works, while maintaining attractive features like single-feed, single-layer and single-radiator properties.

REFERENCES

[1] Guo, J., H. Bai, A. Feng, Y. Liu, Y. Huang, and X. Zhang, "A compact dual-band slot antenna with horizontally polarized omnidirectional radiation," *IEEE Antennas and Wireless Propagation Letters*, Vol. 20, No. 7, 1234–1238, 2021.

[2] Gangwar, S. P., K. Gangwar, and A. Kumar, "Dual band modified circular ring shaped slot antenna for GSM and WiMAX applications," *Microwave and Optical Technology Letters*, Vol. 61, No. 12, 2752–2759, 2019.

[3] Yang, H., Y. Fan, and X. Liu, "A compact dual-band stacked patch antenna with dual circular polarizations for BeiDou navigation satellite systems," *IEEE Antennas and Wireless Propagation Letters*, Vol. 18, No. 7, 1472–1476, 2019.

[4] Nguyen Thi, T., K. C. Hwang, and H. B. Kim, "Dual-band circularly-polarised spidron fractal microstrip patch antenna for ku-band satellite communication applications," *Electronics Letters*, Vol. 49, No. 7, 444–445, 2013.

[5] Saurav, K., D. Sarkar, and K. V. Srivastava, "Dual-band circularly polarized cavity-backed crossed-dipole antennas," *IEEE Antennas and Wireless Propagation Letters*, Vol. 14, 52–55, 2014.

[6] Liang, W., Y.-C. Jiao, Y. Luan, and C. Tian, "A dual-band circularly polarized complementary antenna," *IEEE Antennas and Wireless Propagation Letters*, Vol. 14, 1153–1156, 2015.

[7] Zou, M. and J. Pan, "Wide dual-band circularly polarized stacked rectangular dielectric resonator antenna," *IEEE Antennas and Wireless Propagation Letters*, Vol. 15, 1140–1143, 2015.

[8] Saini, R. K., S. Dwari, and M. K. Mandal, "CPW-fed dual-band dual-sense circularly polarized monopole antenna," *IEEE Antennas and Wireless Propagation Letters*, Vol. 16, 2497–2500, 2017.

[9] Priya, S., K. Kumar, and S. Dwari, "Substrate integrated waveguide dual-frequency dual-sense circularly polarized cavity-backed slot antenna," *International Journal of RF and Microwave Computer-Aided Engineering*, Vol. 29, No. 12, e21987, 2019.

[10] Yue, T., Z. H. Jiang, and D. H. Werner, "A compact metasurface-enabled dual-band dual-circularly polarized antenna loaded with complementary split ring resonators," *IEEE Transactions on Antennas and Propagation*, Vol. 67, No. 2, 794–803, 2019.

[11] Li, J., J. Shi, L. Li, T. A. Khan, J. Chen, Y. Li, and A. Zhang, "Dual-band annular slot antenna loaded by reactive components for dual-sense circular polarization with flexible frequency ratio," *IEEE Access*, Vol. 6, 64 063–64 070, 2018.

[12] Sze, J.-Y. and S.-P. Pan, "Design of CPW-fed circularly polarized slot antenna with a miniature configuration," *IEEE Antennas and Wireless Propagation Letters*, Vol. 10, 1465–1468, 2011.

[13] Saraswat, K. and A. R. Harish, "Dual-band CP coplanar waveguide-fed split-ring resonator-loaded G-shaped slot antenna with wide-frequency ratio," *IET Microwaves, Antennas & Propagation*, Vol. 12, No. 12, 1920–1925, 2018.

[14] Rajgopal, S. K. and S. K. Sharma, "Investigations on ultrawideband pentagon shape microstrip slot antenna for wireless communications," *IEEE Transactions on Antennas and Propagation*, Vol. 57, No. 5, 1353–1359, 2009.

[15] Zhou, S.-W., P.-H. Li, Y. Wang, W.-H. Feng, and Z.-Q. Liu, "A CPW-fed broadband circularly polarized regular-hexagonal slot antenna with L-shape monopole," *IEEE Antennas and Wireless Propagation Letters*, Vol. 10, 1182–1185, 2011.

[16] Singh, A. K., S. Patil, B. K. Kanaujia, and V. K. Pandey, "A novel printed circularly polarized asymmetric wide slot antenna for digital cellular system," *Microwave and Optical Technology Letters*, Vol. 62, No. 3, 1438–1447, 2020.

[17] Yang, W., S. Chen, W. Che, Q. Xue, and Q. Meng, "Compact high-gain metasurface antenna arrays based on higher-mode SIW cavities," *IEEE Transactions on Antennas and Propagation*, Vol. 66, No. 9, 4918–4923, 2018.

[18] Xu, Y., Z. Wang, and Y. Dong, "Circularly polarized slot antennas with dual-mode elliptic cavity," *IEEE Antennas and Wireless Propagation Letters*, Vol. 19, No. 4, 715–719, 2020.

[19] Chen, R.-S., L. Zhu, S.-W. Wong, J.-Y. Lin, Y. Li, L. Zhang, and Y. He, "S-band full-metal circularly polarized cavity-backed slot antenna with wide bandwidth and wide beamwidth," *IEEE Transactions on Antennas and Propagation*, Vol. 69, No. 9, 5963–5968, 2021.

[20] Saraswat, K. and A. R. Harish, "Flexible dual-band dual-polarised CPW-fed monopole antenna with discrete-frequency reconfigurability," *IET Microwaves, Antennas & Propagation*, Vol. 13, No. 12, 2053–2060, 2019.

[21] Birwal, A., S. Singh, B. K. Kanaujia, and S. Kumar, "CPW-fed ultra-wideband dual-sense circularly polarized slot antenna," *Progress In Electromagnetics Research C*, Vol. 94, 219–231, 2019.

[22] Xin, Y., Q. Feng, and J. Tao, "A CPW-fed dual-band slot antenna with circular polarization," *Progress In Electromagnetics Research Letters*, Vol. 61, 77–83, 2016.

[23] Lei, Z.-Y., J. Zhang, R. Yang, X. Liu, L. Chen, and X. Kong, "Design of dual-band dual-sense circularly polarized slot antenna," *Progress In Electromagnetics Research C*, Vol. 43, 41–51, 2013.

[24] Xu, R., J.-Y. Li, J. Liu, D.-J. Wei, K. Wei, Y. X. Qi, and J.-J. Yang, "A very simple dual-band dual-sense circularly polarized square slot antenna," in *2018 IEEE International Symposium on Antennas and Propagation & USNC/URSI National Radio Science Meeting*, 123–124, Boston, MA, USA, 2018.

[25] Wang, M.-S., X.-Q. Zhu, Y.-X. Guo, and W. Wu, "Miniaturized dual-band circularly polarized quadruple inverted-F antenna for GPS applications," *IEEE Antennas and Wireless Propagation Letters*, Vol. 17, No. 6, 1109–1113, 2018.

[26] Lee, C.-H., J.-W. Huang, and C.-I. G. Hsu, "Differentially fed dual-band circularly polarized printed slot antenna with high common-mode rejection," *Microwave and Optical Technology Letters*, Vol. 63, No. 4, 1213–1218, 2021.

[27] Wang, C.-J., M.-H. Shih, and L.-T. Chen, "A wideband open-slot antenna with dual-band circular polarization," *IEEE Antennas and Wireless Propagation Letters*, Vol. 14, 1306–1309, 2015.

[28] Xu, Y., L. Zhu, and N.-W. Liu, "Design approach for a dual-band circularly polarized slot antenna with flexible frequency ratio and similar in-band gain," *IEEE Antennas and Wireless Propagation Letters*, Vol. 21, No. 5, 1037–1041, 2022.

[29] Saini, R. K. and P. S. Bakariya, "Dual-band dual-sense circularly polarized asymmetric slot antenna with F-shaped feed line and parasitic elements," *Progress In Electromagnetics Research M*, Vol. 69, 185–195, 2018.

[30] Bao, X. and M. J. Ammann, "Dual-frequency dual-sense circularly-polarized slot antenna fed by microstrip line," *IEEE Transactions on Antennas and Propagation*, Vol. 56, No. 3, 645–649, 2008.

[31] Sung, Y., "Novel dual-band circularly polarized slot antenna with asymmetrical stubs," *Microwave and Optical Technology Letters*, Vol. 62, No. 12, 3966–3974, 2020.

[32] Kandasamy, K., B. Majumder, J. Mukherjee, and K. P. Ray, "Dual-band circularly polarized split ring resonators loaded square slot antenna," *IEEE Transactions on Antennas and Propagation*, Vol. 64, No. 8, 3640–3645, 2016.

[33] Ge, L., C.-Y.-D. Sim, H.-L. Su, J.-Y. Lu, and C. Ku, "Single-layer dual-broadband circularly polarised annular-slot antenna for WLAN applications," *IET Microwaves, Antennas & Propagation*, Vol. 12, No. 1, 99–107, 2018.

[34] Paul, P. M., K. Kandasamy, and M. S. Sharawi, "A corner expanded slot antenna loaded with copper strips for dual-band circular polarization characteristics," *Microwave and Optical Technology Letters*, Vol. 62, No. 1, 491–497, 2020.

[35] Lee, S., Y. Yang, K.-Y. Lee, and K. C. Hwang, "Dual-band circularly polarized annular slot antenna with a lumped inductor for GPS application," *IEEE Transactions on Antennas and Propagation*, Vol. 68, No. 12, 8197–8202, 2020.

[36] Ji, S., Y. Dong, S. Wen, and Y. Fan, "C/X dual-band circularly polarized shared-aperture antenna," *IEEE Antennas and Wireless Propagation Letters*, Vol. 20, No. 12, 2334–2338, 2021.

[37] Xu, Y., L. Zhu, N.-W. Liu, and M. Li, "A dual-band dual-circularly-polarized slot antenna with stable in-band gain and reduced frequency ratio under triple resonance," *IEEE Transactions on Antennas and Propagation*, Vol. 70, No. 11, 10 199–10 206, 2022.

[38] Jangid, M., J. Jaiverdhan, S. Yadav, and M. M. Sharma, "A CPW fed cross-shaped dual-band circularly polarized monopole antenna with strip/stub/slot resonator loadings," *Progress In Electromagnetics Research M*, Vol. 109, 113–123, 2022.

[39] Wu, Q.-S., Z.-K. Lin, Z.-X. Du, and X. Zhang, "A dual-band dual-sense circularly polarized slot antenna with cascaded non-radiative resonator," *IEEE Antennas and Wireless Propagation Letters*, 1–5, 2024.

[40] Rui, X., J. Li, and K. Wei, "Dual-band dual-sense circularly polarised square slot antenna with simple structure," *Electronics Letters*, Vol. 52, No. 8, 578–580, 2016.

[41] Sze, J.-Y., C.-I. G. Hsu, Z.-W. Chen, and C.-C. Chang, "Broadband CPW-fed circularly polarized square slot antenna with lightening-shaped feedline and inverted-L grounded strips," *IEEE Transactions on Antennas and Propagation*, Vol. 58, No. 3, 973–977, 2010.

[42] Pourahmadazar, J., C. Ghobadi, J. Nourinia, N. Felegari, and H. Shirzad, "Broadband CPW-fed circularly polarized square slot antenna with inverted-L strips for UWB applications," *IEEE Antennas and Wireless Propagation Letters*, Vol. 10, 369–372, 2011.

[43] Balanis, C. A., *Antenna Theory: Analysis and Design*, John Wiley & Sons, 2016.

[44] Zheng, B. and Z. Shen, "Effect of a finite ground plane on microstrip-fed cavity-backed slot antennas," *IEEE Transactions on Antennas and Propagation*, Vol. 53, No. 2, 862–865, 2005.